Mon. Not. R. Astron. Soc. **345,** 539–544 (2003)

Recovery of transverse velocities of steadily rotating patterns in flat galaxies

S. Sridhar[1⋆] and Niranjan Sambhus[2⋆]

[1]*Raman Research Institute, Sadashivanagar, Bangalore 560080, India*
[2]*Astronomisches Institut, Universität Basel, Venusstrasse 7, CH-4102 Binningen, Switzerland*

Accepted 2003 June 27. Received 2003 June 26; in original form 2003 April 16

ABSTRACT

The transverse velocities of steadily rotating, non-axisymmetric patterns in flat galaxies may be determined by a purely kinematic method, using two-dimensional maps of a tracer surface brightness and radial current density. The data maps could be viewed as the zeroth and first velocity moments of the line-of-sight velocity distribution, which is the natural output of integral-field spectrographs. Our method is closely related to the Tremaine–Weinberg method of estimating pattern speeds of steadily rotating patterns, when the tracer surface brightness satisfies a source-free continuity equation. We prove that, under identical assumptions concerning the pattern, two-dimensional maps may be used to recover not just one number (the pattern speed), but the full vector field of tracer flow in the disc plane. We illustrate the recovery process by applying it to simulated data and test its robustness by including the effects of noise.

Key words: galaxies: kinematics and dynamics – galaxies: nuclei.

1 INTRODUCTION

Over the past decade long-slit spectrographs have given way to integral-field spectrographs (IFS), which produce spectra over a fully sampled, two-dimensional region of the sky (see, e.g., Bacon et al. 2001; Thatte et al. 2001; Emsellem & Bland-Hawthorn 2002). These spectral maps (also called the line-of-sight velocity distribution, hereafter LOSVD) contain important information on the flow patterns of non-axisymmetric features in galaxies and their nuclei. It is widely believed that bars and spiral patterns in disc galaxies could influence galaxy evolution through their roles in the transport of mass and angular momentum. These processes are not understood completely, and IFS maps might be expected to play a key role in the construction of dynamical models of evolving galaxies (de Zeeuw 2002; Emsellem 2002). A limitation is that IFS maps provide information about radial, but not transverse, velocities. It is not possible to recover the unmeasured transverse velocities without additional assumptions; a classic example is the modelling of the warped disc of M83, using tilted, circular rings (Rogstad, Lockhart & Wright 1974). However, the flows in non-axisymmetric features, such as bars, are expected to be highly non-circular, and a different approach is needed.

Tremaine & Weinberg (1984, hereafter TW84) considered steadily rotating patterns in flat galaxies, and showed how data from long-slit spectrographs may be used to estimate the pattern speed. Their method assumes that the disc of the galaxy is flat, has a well-defined pattern speed, and that the tracer component obeys a source-free continuity equation. The goal of this paper is to prove that, making identical assumptions concerning the pattern, IFS data can be used to determine not just one number (the pattern speed), but the transverse velocities, and hence the entire two-dimensional vector field of the tracer flow. Like the TW method, one of the strengths of our method is that it is kinematic, and not based on any particular dynamical model. Our main result is equation (8) of Section 2, which provides an explicit expression for the transverse component of the tracer current in the disc plane, in terms of its surface brightness and the radial current density maps on the sky. This formula is applied in Section 3 to a model of the lopsided disc in the nucleus of the Andromeda galaxy (M31), where we also discuss the effects of noise on the data maps. Section 4 offers conclusions.

2 THE RECOVERY METHOD

An IFS data set consists of a two-dimensional map of the luminosity-weighted distribution of radial velocities, the LOSVD. The LOSVD can be regarded as a function of the three variables, (X, Y, U), where X and Y are Cartesian coordinates on the sky, and U is the radial velocity. The zeroth moment of the LOSVD over U is $\Sigma_{\rm sky}(X, Y)$, the surface brightness distribution on the sky, and the first moment is $F_{\rm sky}(X, Y)$, the radial current density on the sky.[1] Following TW84, we consider a thin disc that is confined to the $z = 0$ plane, with x and y being Cartesian coordinates in the disc plane. The disc is inclined at an angle i to the sky plane ($i = 0^\circ$ is

⋆E-mail: ssridhar@rri.res.in (SS); sambhus@astro.unibas.ch (NS).

[1] The mean radial velocity is then given by $\overline{U}(X, Y) = (F_{\rm sky}/\Sigma_{\rm sky})$: the contour map of $\overline{U}(X, Y)$ is often referred to as a 'spider diagram'.

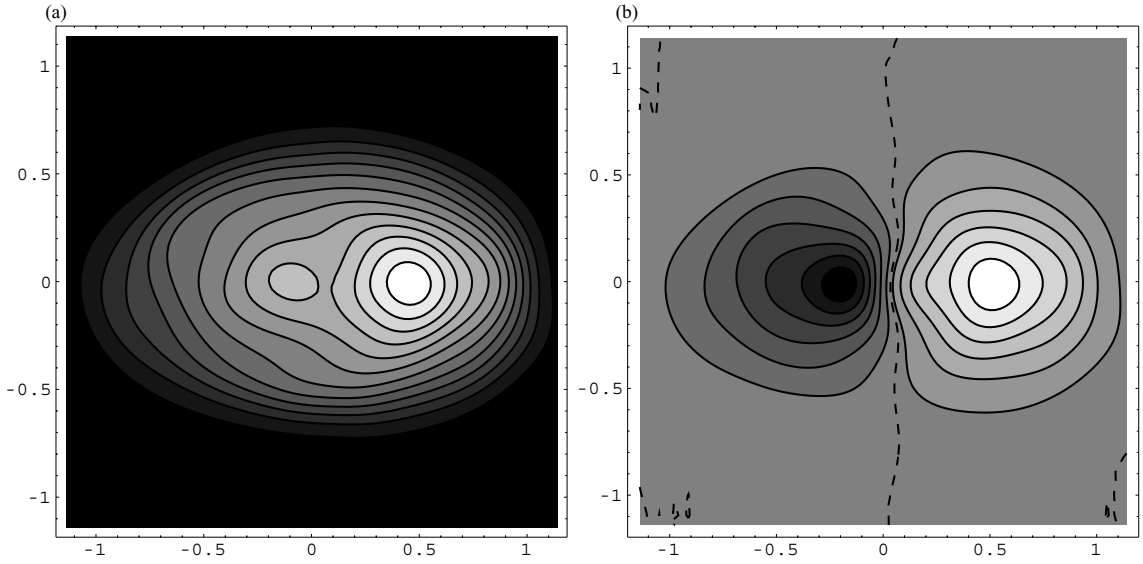

Figure 1. Simulated data from a model disc inclined at 51°.54: two-dimensional distribution of (a) surface brightness ($\Sigma_{\rm sky}$) and (b) radial current density ($F_{\rm sky}$) of the model disc. The images have been smoothed with a circular Gaussian beam ($\sigma = 0.1$ arcsec). The contour levels are arbitrary, but separated uniformly in the values of $\Sigma_{\rm sky}$ and $F_{\rm sky}$, respectively. In (b) the black and white shading corresponds to negative and positive radial current densities, and the dashed line is the zero radial current density contour. In both maps, the line of nodes is along the x-axis. The axes scales are in arcsec. ('Data' taken from SS02.)

face-on and $i = 90^\circ$ is edge-on), with line of nodes coincident with the x-axis. It is clear that the sky coordinates, (X, Y), may be oriented such that the X-axis and x-axis are coincident. Then $(X, Y) = (x, y\cos i)$.

The non-axisymmetric pattern of the tracer is assumed to rotate steadily at an angular rate $\Omega_{\rm p}\hat{z}$. In this frame the continuity equation for the tracer brightness assumes its simplest form. Let $\boldsymbol{r}$ be the position vector in the rotating frame, $\Sigma(\boldsymbol{r})$ be the tracer surface brightness, and $\boldsymbol{v}(\boldsymbol{r})$ be the streaming velocity field in the inertial frame. An observer in the rotating frame sees the tracer move with velocity $[\boldsymbol{v}(\boldsymbol{r}) - \Omega_{\rm p}(\hat{\boldsymbol{z}} \times \boldsymbol{r})]$. If the tracer brightness is conserved, Σ and $(\Sigma\boldsymbol{v})$ must obey the continuity equation, $\boldsymbol{\nabla}\cdot[\Sigma(\boldsymbol{v} - \Omega_{\rm p}\,\hat{\boldsymbol{z}}\times\boldsymbol{r})] = 0$. Cartesian coordinates in the rotating frame may be chosen such that they coincide instantaneously with the (x, y) axis; thus $\boldsymbol{r} = (x, y)$ and $\boldsymbol{v}(\boldsymbol{r}) = (v_x, v_y)$. In component form, the continuity equation reads as

$$\frac{\partial(\Sigma v_x)}{\partial x} + \frac{\partial(\Sigma v_y)}{\partial y} = \Omega_{\rm p}\left(x\frac{\partial\Sigma}{\partial y} - y\frac{\partial\Sigma}{\partial x}\right), \tag{1}$$

which is equivalent to equations (2) and (3) of TW84. The quantities, $\Sigma(x, y)$ and $\Sigma(x, y)v_y(x, y)$, can be related directly to the observed surface brightness and radial current density maps:

$$\Sigma(x, y) = \cos i\,\Sigma_{\rm sky}(X, Y), \tag{2}$$

$$\Sigma(x, y)v_y(x, y) = \cot i\,F_{\rm sky}(X, Y). \tag{3}$$

Henceforth $\Sigma(x, y)$ and $\Sigma(x, y)v_y(x, y)$ will be considered as known quantities. The unknowns in equation (1) are $\Omega_{\rm p}$ and $\Sigma(x, y)v_x(x, y)$. Below we prove that both quantities may be obtained by integrating over x. We will assume that $\Sigma(x, y)$, $\Sigma(x, y)v_y(x, y)$, and (the unknown quantity) $\Sigma(x, y)v_x(x, y)$, all decrease sufficiently rapidly with distance, such that all the integrals encountered below are finite.

Integrating equation (1) over x from $-\infty$ to x, we obtain

$$\Sigma(x, y)v_x(x, y) = -\frac{\partial}{\partial y}\int_{-\infty}^{x} {\rm d}x'\left(\Sigma v_y - \Omega_{\rm p}x'\Sigma\right)_{(x', y)} - \Omega_{\rm p}y\Sigma(x, y), \tag{4}$$

where we have used $\Sigma(-\infty, y) = 0$ and $\Sigma(-\infty, y)v_x(-\infty, y) = 0$. We must also require that $\Sigma(+\infty, y) = 0$, and $\Sigma(+\infty, y)v_x(+\infty, y) = 0$. This leads to the condition

$$\frac{\partial}{\partial y}\int_{-\infty}^{+\infty} {\rm d}x(\Sigma v_y - \Omega_{\rm p}x\Sigma) = 0. \tag{5}$$

Since the integral in equation (5) is independent of y, we can infer its value at large values of $|y|$. Therefore, the integral itself must vanish, i.e.

$$\Omega_{\rm p}\int_{-\infty}^{+\infty} {\rm d}x\,x\Sigma(x, y) = \int_{-\infty}^{+\infty} {\rm d}x\,\Sigma(x, y)v_y(x, y), \tag{6}$$

for *any* value of y. This will be recognized as the key relation that TW84 employ to determine the pattern speed (see equation 5 of their paper). As is clear from our derivation, the real significance of equation (6) is that $\Omega_{\rm p}$ is an *eigenvalue* of equation (4). In other words, it provides a consistency condition that $\Sigma(x, y)$ and $\Sigma(x, y)v_y(x, y)$ must satisfy, if $\Sigma(x, y)v_x(x, y)$ is to be given by equation (4). Using equation (3), we can rewrite equations (6) and (4), such that $\Omega_{\rm p}$ and $\Sigma(x, y)v_x(x, y)$ are expressed directly in terms of observed quantities:[2]

$$\Omega_{\rm p}\sin i\int_{-\infty}^{+\infty} {\rm d}X\,X\Sigma_{\rm sky}(X, Y) = \int_{-\infty}^{+\infty} {\rm d}X\,F_{\rm sky}(X, Y), \tag{7}$$

$$(\Sigma v_x)_{(x,y)} = -(\cos i)^2\frac{\partial}{\partial Y}\int_{-\infty}^{X} {\rm d}X'\left(\frac{F_{\rm sky}}{\sin i} - \Omega_{\rm p}X'\Sigma_{\rm sky}\right)_{(X', Y)} - \Omega_{\rm p}Y\Sigma_{\rm sky}(X, Y). \tag{8}$$

In the next section, equations (7) and (8) will be used on the simulated data of Fig. 1, to enable recovery of the entire two-dimensional flow vector field of a steadily rotating, lopsided pattern.

[2] In principle, the value of $\Omega_{\rm p}$ given by equation (7) should be independent of Y. However, TW84 recommends multiplying equation (7) by some weight function, $h(Y)$ and integrating over Y, to obtain an estimate of $\Omega_{\rm p}$ as the ratio of two integrals – see equation (7) of TW84.

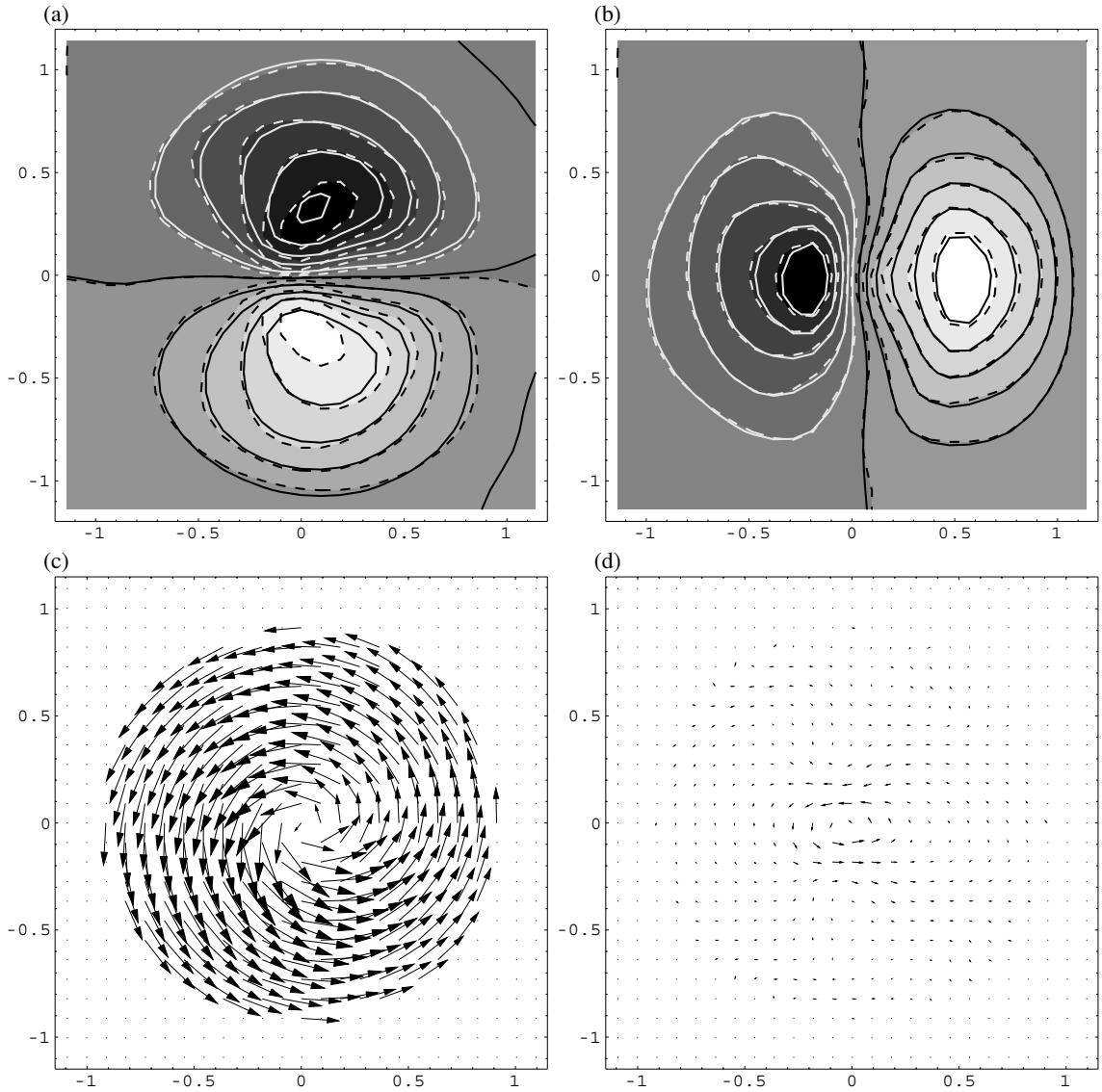

Figure 2. (a) and (b) display isocontours of the *x*- and *y*-current densities, respectively, in the disc plane. The contour levels are equally spaced in current units. The continuous and dashed curves correspond to the recovered and model current densities, respectively. The black and white shadings correspond to negative and positive current densities. The velocity field of the input model is shown in (c). The recovered velocity field is close to the input model, and we show only the residuals (i.e. recovered minus model velocities) in (d). All axes are in arcsec.

3 APPLICATION TO SIMULATED DATA

We used as data, simulated observations of a numerical model of the stellar disc in the nucleus of the Andromeda galaxy (M31). A brief account of the model is given below, and the reader is referred to Sambhus & Sridhar (2002, hereafter SS02) for details. The nucleus of M31 is believed to harbour a supermassive black hole (SMBH, Kormendy & Bender 1999), surrounded by a dense stellar disc, which appears as a lopsided, double-peaked structure (Lauer et al. 1993). The two peaks are separated by about 0.5 arcsec, with the fainter peak almost coincident with the location of the SMBH (Lauer et al. 1998). The dynamical centre of the galaxy lies in between the two peaks, about 0.1 arcsec from the SMBH. Tremaine (1995) proposed that the SMBH was surrounded by an eccentric disc of stars, for which the orbital apoapsides were aligned in a manner that gave rise to the lopsided peak in the density of stars. Our input model is a dynamical model of this eccentric disc that was constructed by SS02, based on the *Hubble Space Telescope* photometry of Lauer et al. (1998). The model consisted of about 230 000 points distributed on a plane. Each point ('star') possessed five attributes: luminosity (or mass), location in the plane and two components of velocity. The lopsided pattern formed by these points rotated steadily about an axis normal to the plane with a (prograde) pattern speed equal to 16 km s^{-1} pc^{-1}; thus the model satisfied all the assumptions used in Section 2. SS02 estimated an inclination angle $i = 51\overset{\circ}{.}54$, and we use this value while projecting the model disc to the sky-plane. To obtain a smooth distribution, we 'observed' the model with a circular Gaussian beam of $\sigma = 0.1$ arcsec. Fig. 1 shows the surface brightness ($\Sigma_{\rm sky}$) and the radial current density ($F_{\rm sky}$). The line of nodes is along the *x*-axis.

We computed the integrals in equation (7), using $\Sigma_{\rm sky}$ and $F_{\rm sky}$ from Fig. 1, for 11 different values of Y. Following Gerssen, Kuijken & Merrifield (1999), we plotted the 11 different values of one integral against the 11 values of the other integral. The slope

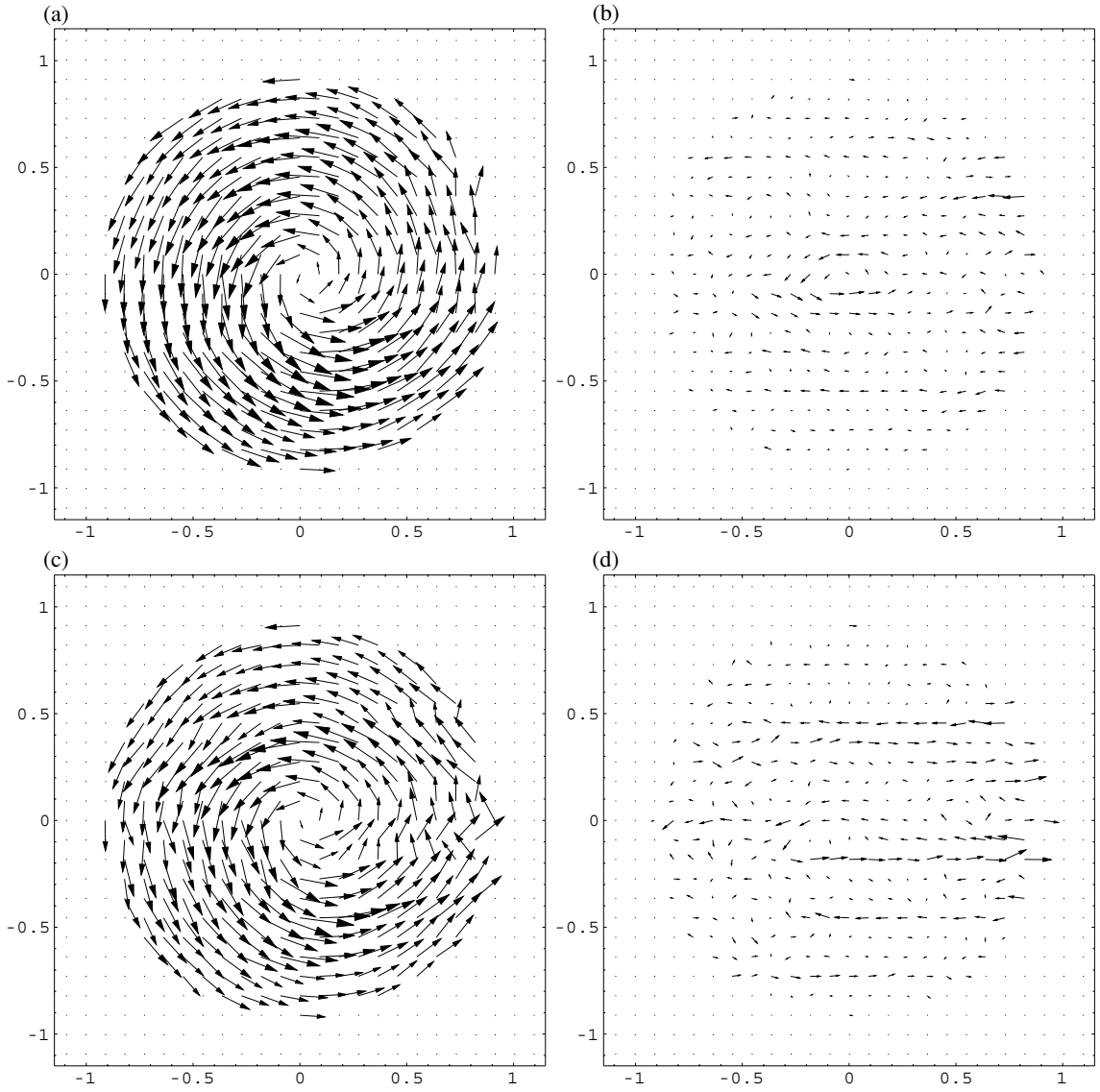

Figure 3. Recovered velocity fields and residuals for typical noisy realizations. (a) and (c) are the recovered velocity fields for noise levels of 5 and 10 per cent, respectively. (b) and (d) are the respective residuals.

of the 'best-fitting' straight line (in the least-square sense) gave an estimate of $\Omega_{\rm p} \sin i$. Using $i = 51^{\circ}.54$, we found that $\Omega_{\rm p} = 15.11 \pm 0.47$ km s^{-1} pc^{-1}. We used this value of $\Omega_{\rm p}$ to compute the right-hand side of equation (8). After deprojection using $(x, y) = (x, y \cos i)$ we obtained the x-current density (Σv_x), the isocontours of which are displayed in Fig. 2(a) as the continuous curves. For comparison, we also plot the isocontours of (Σv_x) from the input model in the same figure as the dashed curves. In Fig. 2(b) similar plots of (Σv_y) are displayed to make the point that, in practice, deprojection can also give rise to errors. It is traditional and useful to look at the velocity field, instead of the current density field. The velocity field is obtained by dividing the current density field by $\Sigma(x, y)$, and we may expect this process of division to give rise to errors, especially in the outer parts where Σ is small. To quantify the errors, we computed the residual map, which was defined as the difference between the recovered and input x-velocity maps. The Σ-weighted mean (R) and root-mean-squared (rms; σ_R) values of the residual map were then calculated. When expressed in units of $|v_x|_{\rm max}$ of the input map, they were found equal to $R = 1.09\times 10^{-3}$ and $\sigma_R = 7.67 \times 10^{-2}$. These globally determined numbers should give the reader some idea of the dynamic range of the recovery method, when applied to noise-free spatially smoothed data. The spatial distribution of the errors in both the x and y velocities is best visualized with 'arrow plots' of the velocity fields. Fig. 2(c) displays the velocity field of the input model in the disc plane. The reconstructed velocities are close to the model, and we do not present them separately. Instead we plot the residual current field (recovered minus input) in Fig. 2(d).

We also tested the recovery method on noisy data. In a real observation most of the error is likely to reside in the measurement of velocities, rather than the surface brightness. This is because the methods used to extract the velocity information from spectra are less robust than photometry. Therefore, we added noise to Fig. 1(b), and kept Fig. 1(a) noise-free. To each pixel of Fig. 1(b), we added

Table 1. Column 1: noise level added to 'observed' radial velocity map. The quantities in columns 2–4 were obtained by averaging over 21 realizations for each level of noise. Column 2: pattern speed from using equation (7), in units of km s^{-1} pc^{-1}. Columns 3 and 4: mean and rms residuals of recovered transverse velocities, respectively, in units of $|v_x|_{\max}$ of the input map.

Noise	$\Omega_{\rm p}$ (error)	$\overline{R}$ (error)	$\overline{\sigma_R}$ (error)
1 per cent	15.29 (0.79)	1.14×10^{-3} (1.75×10^{-4})	8.02×10^{-2} (1.54×10^{-3})
5 per cent	17.67 (3.24)	1.50×10^{-3} (6.69×10^{-4})	1.30×10^{-1} (1.45×10^{-2})
10 per cent	16.78 (6.38)	1.00×10^{-3} (1.22×10^{-3})	2.30×10^{-1} (3.42×10^{-2})

Gaussian noise with mean equal to that observed, and rms equal to some fixed fraction of the mean.[3] We experimented with three levels of noise, namely rms noise per pixel equal to 1, 5 and 10 per cent of the mean. For each level of noise, 21 realizations were explored. The pattern speed, x-current density and x velocities were computed for each realization, using equations (7) and (8). Comparing with the input model, we computed the mean (R) and rms (σ_R) of the residual x velocities for each realization. The distributions of the 21 R and σ_R values were peaked close to their mean values, $\overline{R}$ and $\overline{\sigma_R}$, respectively. Table 1 provides estimates (and rms errors) for these, as well as for the pattern speed.

The mean residual, $\overline{R}$, is always quite small, implying that there is very little global systematic shift in the x velocities. This occurs because of cancellation between positive and negative residual velocities. The estimated pattern speed is also well behaved, because this is calculated using numbers from different Y cuts. However, the errors on $\Omega_{\rm p}$ increase dramatically with noise, resulting in a significant increase in $\overline{\sigma_R}$. As earlier, the arrow plots are very revealing. The recovered and residual maps for the case of 1 per cent noise are very close to the noise-free case discussed earlier. Therefore, in Fig. 3 we display arrow plots only for noise levels of 5 and 10 per cent. In addition to random errors in the residual velocities there are systematic alignments parallel to the line of nodes, the axis along which integrals are evaluated in the recovery method. However, as Fig. 3 suggests, even for a noise level as high as 10 per cent, the recovery method does not fail completely.

4 CONCLUSIONS

We have demonstrated that it is possible to recover the transverse velocities of steadily rotating patterns in flat galaxies, using two-dimensional maps of a tracer surface brightness and radial current density, if the tracer satisfies a source-free continuity equation. Our method is kinematic, and closely related to the TW method of determining pattern speeds. Indeed, the conditions that need to be satisfied – that the galaxy is flat, the pattern is steadily rotating and the tracer obeys a continuity equation – are identical to those assumed by TW84. Our main result is an explicit expression for the transverse velocities (equation 8), which is exact under ideal conditions. We have applied it successfully to simulated data, and demonstrated its utility in the presence of intrinsic numerical errors in the data, finite angular resolution, and noise. The TW relation for the pattern speed (equation 7) emerges as an eigenvalue, and we expect our method to work well whenever the TW method gives a good estimate of the pattern speed. It is legitimate to be concerned that the conditions required to be satisfied might impose serious limitations in practice; the angle of inclination and line of nodes need to be estimated, the pattern need not be steadily rotating, the continuity equation need not be satisfied, the tracer distribution could be warped, the disc could be thick, and there could be streaming velocities in the z-direction. All of these are well-known worries concerning the applicability of the TW method itself. That they are not unduly restrictive is evident from the success that the TW method itself has enjoyed in the determination of pattern speeds (see, e.g., Kent 1987; Kuijken & Tremaine 1991; Merrifield & Kuijken 1995; Bureau et al. 1999; Gerssen, Kuijken & Merrifield 1999; Baker et al. 2001; Debattista & Williams 2001; Debattista, Corsini & Aguerri 2002a; Debattista, Gerhard & Sevenster 2002b; Gerssen 2002; Zimmer & Rand 2002; Aguerri, Debattista & Corsini). Therefore, we are cautiously optimistic that our method of recovering transverse velocities can be applied usefully to two-dimensional spectral maps.

[3] Adding noise to $F_{\rm sky}$ is equivalent to adding noise to $\overline{U} = (F_{\rm sky}/\Sigma_{\rm sky})$, because we have kept $\Sigma_{\rm sky}$ noise-free.

ACKNOWLEDGMENTS

We are grateful to D. Bhattacharya, E. Emsellem, V. Radhakrishnan, and in particular to an anonymous referee for very helpful comments and suggestions. NS was supported by grant 20-64856.01 of the Swiss National Science Foundation.

REFERENCES

Aguerri J.A.L., Debattista Victor P., Corsini E.M., 2003, MNRAS, 338, 465
Bacon R. et al., 2001, MNRAS, 326, 23
Baker A.J., Schinnerer E., Scoville N.Z., Englmair P.P., Tacconi L.J., Tacconi-Garman L.E., Thatte N., 2001, in Knapen J.H., Beckman J.E., Schlosman I., Mahoney T.J., eds, ASP Conf. Ser. Vol. 249, The Central Kiloparsec of Starbursts and AGN: the La Palma Connection. Astron. Soc. Pac., San Fransisco, p. 78
Bureau M., Freeman K.C., Pfitzner D.W., Meurer G.R., 1999, AJ, 118, 2158
Debattista V.P., Williams T.B., 2001, in Funes J.G., Corsini S.J., Corsini E.M., eds, ASP Conf. Ser. 230, Galaxy Disks and Disk Galaxies. Astron. Soc. Pac., San Fransisco, p. 553
Debattista V.P., Corsini E.M., Aguerri J.A.L., 2002a, MNRAS, 332, 65
Debattista V.P., Gerhard O., Sevenster M.N., 2002b, MNRAS, 334, 355
de Zeeuw T., 2002, in Sembach K.R., Blades J.C., Illingworth G.D., Kennicutt R.C., eds, ASP Conf. Ser., Hubble's Science Legacy: Future Optical–Ultraviolet Astronomy from Space. Astron. Soc. Pac., San Francisco, in press (astro-ph/0209114)
Emsellem E., 2002, in Athanassoula E., Bosma A., Mujica R., eds, ASP Conf. Ser. 275, Disks of Galaxies: Kinematics, Dynamics and Perturbations. Astron. Soc. Pac., San Fransisco, p. 255
Emsellem E., Bland-Hawthorn J., 2002, in Rosado M., Binette L., Arias L., eds, ASP Conf. Ser. Vol. 282, Galaxies, the Third Dimension. Astron. Soc. Pac., San Francisco, p. 539
Gerssen J., 2002, in Athanassoula E., Bosma A., Mujica R., eds, ASP Conf. Ser. 275, Disks of Galaxies: Kinematics, Dynamics and Perturbations. Astron. Soc. Pac., San Fransisco, p. 197

Gerssen J., Kuijken K., Merrifield M.R., 1999, MNRAS, 306, 926
Kent S.M., 1987, AJ, 93, 1062
Kormendy J., Bender R., 1999, ApJ, 522, 772
Kuijken K., Tremaine S., 1991, in Sundelius B., ed., Dynamics of Disc Galaxies. Göteborg Univ, Göteborg, p. 71
Lauer T.R. et al., 1993, AJ, 106, 1436
Lauer T.R., Faber S.M., Ajhar E.A., Grillmair C.J., Scowen P.A., 1998, AJ, 116, 2263
Merrifield M.R., Kuijken K., 1995, MNRAS, 274, 933
Rogstad D.H., Lockhart I.A., Wright M.C.H., 1974, ApJ, 193, 309
Sambhus N., Sridhar S., 2002, A&A, 388, 766 (SS02)
Thatte N., Eisenhauer F., Tecza M., Mengel S., Genzel R., Monnet G., Bonaccini D., Emsellem E., 2001, in Kaper L., van den Heuvel E.P.J., Woudt P.A., eds, Proc. ESO Workshop, Black Holes in Binaries and Galactic Nuclei. Springer-Verlag, Berlin, p. 107
Tremaine S., 1995, AJ, 110, 628
Tremaine S., Weinberg M., 1984, ApJ, 282, L5 (TW84)
Zimmer P., Rand R., 2002, AAS meeting, 200, 97.01

This paper has been typeset from a TEX/LATEX file prepared by the author.